PROCEEDINGS PREPRINT

SPIE–The International Society for Optical Engineering

Preprinted from

Laser Techniques for State-Selected and State-to-State Chemistry II

From Session 5:

Laser Diagnostics for Combustion

Volume 2124

27–29 January 1994
Los Angeles, California

Laser Imaging of Chemistry-Flowfield Interactions: Enhanced Soot Formation in Time-Varying Diffusion Flames

Joel E. Harrington[a], Christopher R. Shaddix[b], and Kermit C. Smyth

Building and Fire Research Laboratory
National Institute of Standards and Technology
Gaithersburg, MD 20899

ABSTRACT

Models of detailed flame chemistry and soot formation are based upon experimental results obtained in steady, laminar flames. For successful application of these descriptions to turbulent combustion, it is instructive to test predictions against measurements in time-varying flowfields. This paper reports the use of optical methods to examine soot production and oxidation processes in a co-flowing, axisymmetric CH_4/air diffusion flame in which the fuel flow rate is acoustically forced to create a time-varying flowfield. For a particular forcing condition in which tip clipping occurs (0.75 V loudspeaker excitation), elastic scattering of vertically polarized light from the soot particles increases by nearly an order of magnitude with respect to that observed for a steady flame with the same mean fuel flow rate. The visible flame luminosity and laser-induced fluorescence attributed to polycyclic aromatic hydrocarbons (PAH) are also enhanced. Peak soot volume fractions, as measured by time-resolved laser extinction/tomography at 632.8 and 454.5 nm and calibrated laser-induced incandescence (LII), show a factor of 4–5 enhancement in this flickering flame. The LII method is found to track the soot volume fraction closely and to give better signal-to-noise than the extinction measurements in both the steady and time-varying flowfields. A Mie analysis suggests that most of the enhanced soot production results from the formation of larger particles in the time-varying flowfield.

1. INTRODUCTION

Gas phase combustion involves complex interactions between chemical and transport processes in even the simplest steady laminar flames. The development of comprehensive and detailed descriptions of flame structure and the formation of pollutants, such as NO and smoke, has relied upon comparisons of model predictions with experimental data obtained in simplified flame systems. A critical assumption in applying these chemical models to turbulent combustion is that the limited combinations of residence times, temperature histories, local stoichiometries, and strain rates sampled in laboratory-scale steady laminar flames are sufficient to quantitatively describe the key chemical processes in turbulent environments. In order to critically evaluate the validity of this assumption, an experimental facility for performing optical measurements in time-varying, laminar diffusion flames has been developed at NIST [1]. This apparatus allows the time-dependent interaction of variable-strength external vortex rings with the flame structure to be investigated systematically.

[a] Present address: SRI International, Molecular Physics Laboratory, Menlo Park, CA 94025.
[b] National Research Council NIST Postdoctoral Research Associate 1993 - present.

Under a wide variety of conditions, axisymmetric diffusion flames and pool fires exhibit a natural flickering behavior, with a frequency dependence on the fuel tube or pool diameter expressed as $f \sim 1.5/(D)^{1/2}$ (for f in Hz and D in meters) [2,3]. This flickering results from the cyclical formation and convection of vortex rings external to the flame sheet [4–6]. The large vortical structures apparently form due to a Kelvin-Helmholtz type of hydrodynamic instability which arises from the buoyant acceleration of the high-temperature, low-density gases and the resulting shear with the more slowly moving coflow [5–7]. Previous researchers have found that the flickering tendency may be locked near the natural flicker frequency by applying a small periodic perturbation to the fuel flow [8-11]. In the present investigation optical diagnostics are phase-locked to a sinusoidal variation of the fuel flow velocity at the 10 Hz repetition rate of a Nd^{3+}:YAG laser, allowing phase-specific measurements to be made.

Soot formation is an important process which is especially sensitive to the local combustion conditions, since the pre-particle soot inception chemistry is relatively slow [12]. The local temperature, residence time, and mixture fraction have been identified as important variables in soot production, in addition to the chemical structure of the fuel. One might anticipate that chemistry-flowfield interactions will have a significant impact upon soot formation, and indeed our experimental results reveal that soot production increases dramatically in flickering CH_4/air flames.

In a preliminary study of OH· laser-induced fluorescence and elastic scattering from soot in steady and time-varying CH_4/air diffusion flames, it was found that the scattering intensity in the time-varying flame is much greater than that observed for the steady (i.e., unforced) flame with the same mean fuel and air flow rates [1]. Figure 1 presents some of these results to aid in the interpretation of the experiments described below. Images of OH· laser-induced fluorescence and soot scattering are shown for the flickering flame and its steady counterpart. The OH· fluorescence signals have not been corrected for local quenching rates and hence serve as a convenient, qualitative marker of the high-temperature reaction zone.

In order to better quantify the observed soot enhancement for a forcing condition in which flame tip clipping occurs, we have applied laser light extinction and laser-induced incandescence (LII) to determine the soot volume fraction fields in these CH_4/air flames [13]. In addition, laser energy-corrected imaging of soot scattering in the steady and flickering flame has been performed using vertically polarized incident light, supplementing previous work using horizontal polarization [1]. Measurements have also been made of visible flame luminosity, which is an indicator of the total soot radiation, and broadband laser-induced fluorescence attributed to polycyclic aromatic hydrocarbons (PAH). Radiation from soot dominates energy transfer in practical fires, and PAH species are likely soot precursors.

2. EXPERIMENTAL METHODS

Methane has been chosen as the fuel since steady laminar CH_4/air diffusion flames have been investigated extensively in our laboratory (Ref. 14 compares our results with flame structure calculations), and CH_4/air flames are also widely used in current attempts to include realistic hydrocarbon chemistry in turbulent flows with either flamelet libraries or reduced chemical mechanisms [15]. Figure 2 shows a schematic diagram of the burner and phase-locked imaging setup, which has been described in detail previously [1]. A coannular axisymmetric burner with a 1.1 cm diameter fuel tube surrounded by a 10.2 cm air annulus supports an unconfined laminar flame. The mean methane cold flow fuel velocity and air coflow are 7.9 cm/s for both the steady and forced flames; the steady flame has a visible height of 79 mm. A loudspeaker attached to the fuel plenum locks the frequency of the flickering flame to the 10.13 Hz

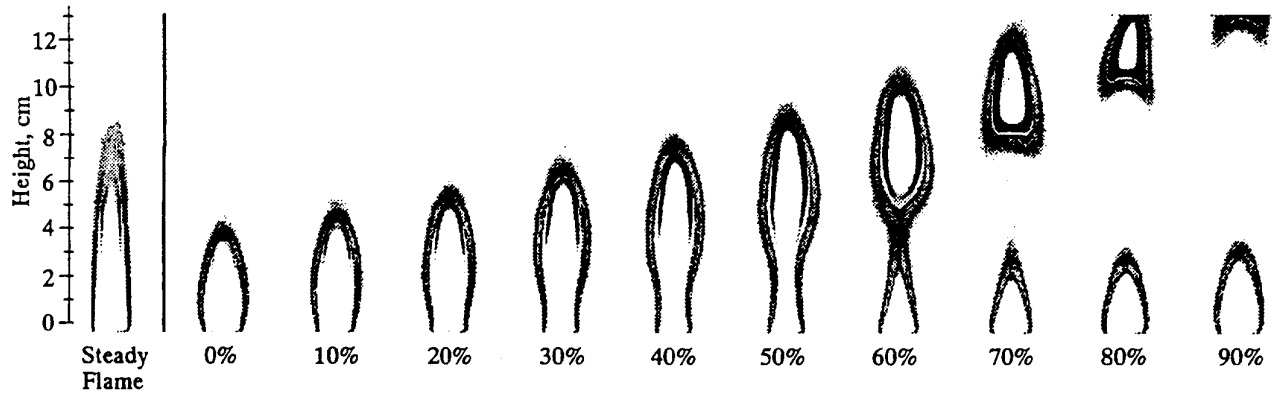

Figure 1. Laser energy-corrected OH• laser-induced fluorescence and soot scattering images in a steady and time-varying laminar CH_4/air diffusion flame using horizontally polarized light at 283.55 nm. The visible flame height of the steady flame is 79 mm above the fuel tube exit, which is located 1 mm above the bottom of the images. For the flickering flame, ten equally spaced phase increments are shown, corresponding to a time interval of 10 ms; the zero phase is arbitrary. For the full-height images presented here, five single-shot images (3.2 cm high) have been overlapped to compensate for reduced signal-to-noise at the upper and lower edges of the incident laser sheet. Several of the stacked images shown have been shifted slightly from side-to-side to compensate for flame wobble at higher flame locations.

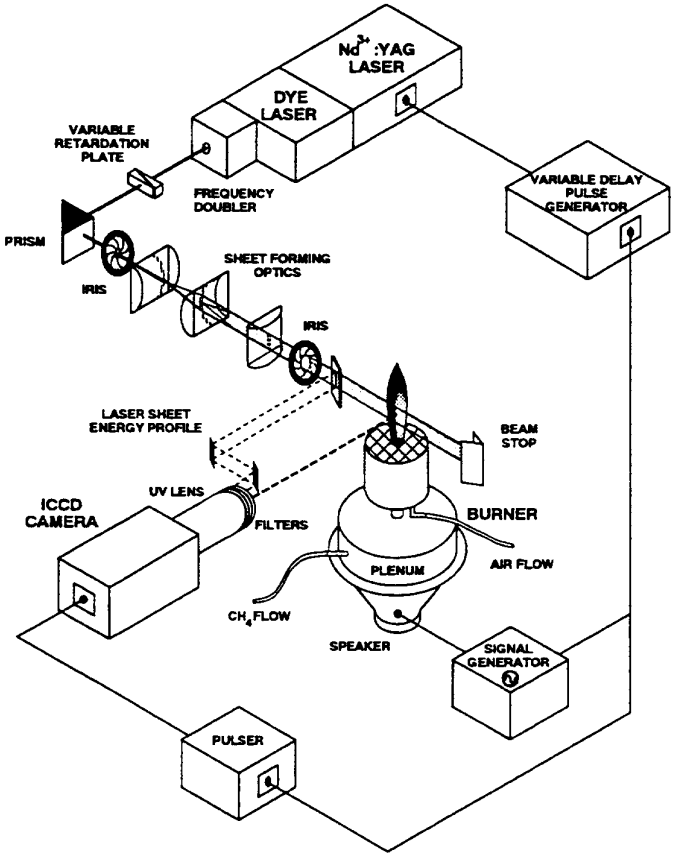

Figure 2. Experimental set-up for 1- or 2-D imaging of axisymmetric diffusion flames which are acoustically excited and phase-locked to the pulsed dye laser system operating at 10.13 Hz. For the laser-induced incandescence experiment, the frequency doubler and sheet-forming optics are removed, and a 300 mm focal length lens is used to focus the beam at the center of the flame. Images are recorded using an intensified charge-coupled device (ICCD) camera.

repetition rate of the Nd^{3+}:YAG pumped dye laser system. The flickering flame data presented here were taken with 0.75 V peak-to-peak sine wave forcing, which is an intermediate excitation amplitude of those studied earlier [1].

2.1 Laser extinction

Laser light extinction has traditionally been used to measure soot volume fraction. However, both absorption from large molecules, such as polycyclic aromatic hydrocarbons (PAH), and soot scattering interfere with the signal from soot absorption. For the CH_4/air flames studied here, soot scattering should represent a minor portion of the extinction, since the primary soot particles are small [16] and the extent of soot agglomeration in our relatively short residence time flames is expected to be limited. On the other hand, the contribution of molecular absorption to the measured extinction is of concern, particularly at low soot loadings. Consequently, extinction measurements were performed using the longest wavelength cw laser readily available in our laboratory (632.8 nm - HeNe). In most cases extinction was also measured using a shorter wavelength laser source (454.5 nm - Ar^+), where molecular absorption is expected to be much stronger [17].

In order to perform accurate extinction measurements in these lightly sooting flames, a laser power stabilizer was used to reduce the noise in the input laser beams to ~ 0.1%, allowing measurement of extinction levels as small as 0.01% after averaging. Small beam movements from thermal lensing on the detector photodiode were an important error source unless minimized through 1-to-1 imaging of the flame centerline, using a lens between the flame and diode. This imaging approach was recommended by Montgomery and Reuss [18] in their flame holography studies. The line-of-sight nature of extinction necessitates data collection along multiple chords and subsequent tomographic inversion to yield locally resolved values of extinction. To obtain acceptable signal-to-noise, 200 consecutive time records of the amplified photodiode output were averaged using a digital oscilloscope. Extinction records were obtained for radial chords spaced by 0.25 mm across the width of the flames and were tomographically inverted with a 3-point Abel routine as implemented by Dasch [19]. For the time records in the flickering flame a Pascal-encoded version of Dasch's routine [20] was employed to yield phase-specific extinction profiles.

2.2 Laser-induced incandescence

Laser-induced incandescence (LII) has recently been developed as an alternative method for both relative [21,22] and quantitative [23] measurement of soot volume fraction. We employed LII as a second means of quantifying the soot volume fraction in both the steady and flickering CH_4/air flames in order to identify possible contributions from molecular absorption to the measured extinction and to avoid noise difficulties in the extinction signal which arose from flame wobble at heights above 60 mm in the flickering flame. For the LII measurement the fundamental dye laser beam at 560 nm was focused with a 300 mm focal length lens at the center of the flame. In order to minimize signal variations with shot-to-shot laser energy fluctuations, the LII data were obtained at sufficiently high energies (~ 7×10^8 W/cm^2) to lie well within the plateau region where the LII signal varies little with laser energy [22,23]. Single-shot, 1-D line images were recorded on the ICCD camera, with a glass filter providing a detection bandwidth of 300–480 nm. Flame luminosity signals were ~ 10 times weaker than the LII signals and were accounted for by taking a duplicate set of line images without laser light and subtracting these from the LII images. Further experimental details of the extinction and LII measurements are given in Ref. 13.

2.3 Soot scattering

Scattering measurements were made with the same basic experimental setup and data collection procedure used for the earlier OH· and soot imaging, in which dye laser light at 567 nm was frequency doubled to 283.5 nm [1]. To image scattering using vertically polarized light, a variable retardation plate (Babinet-Soleil compensator) rotated the incident beam to a vertical polarization relative to the detection axis. Shot-to-shot spatial profiles of the laser energy were recorded via on-camera imaging of a reflection from the incident laser sheet (see Fig. 2).

2.4 PAH laser-induced fluorescence

Broadband laser-induced fluorescence, presumably from PAH molecules, was excited at a laser wavelength of 283.5 nm and detected using a short-pass dielectric filter with a bandpass of 415-550 nm. This filter effectively blocked scattered light from the soot particles. Earlier work on excitation of this broadband fluorescence using UV radiation showed evidence for two PAH populations, which can be distinguished by their spatial profiles and to a limited degree by the wavelength of their emission [24]. Prior to the imaging experiments the laser energy dependence of the fluorescence from both components was measured and exhibited evidence of partial optical saturation for fluence levels slightly lower than that required for partial saturation of the $S_{21}(8)$ transition in the OH· $A^2\Sigma^+ \leftarrow X^2\Pi_i$ (1,0) band. For a laser fluence sufficiently low to avoid optical saturation of the PAH fluorescence, the observed signals were too weak to obtain single-shot images with reasonable signal-to noise. Therefore, higher laser energies were used, with care taken to avoid laser-induced incandescence from the soot particles. The broadband fluorescence data shown in the next section were selected from the 2-D images in the steady and flickering flames at locations of equal laser energy. As with the LII data, background luminosity was subtracted from the broadband fluorescence images.

2.5 Flame luminosity

Visible radiation from the soot particles was measured using a wide 3 μs gate on the ICCD camera and the 415-550 nm bandpass dielectric filter. Unlike the one- and two-dimensional laser images, the luminosity signals arise from all regions of the flame containing soot. Most of the light is collected from the image plane at the flame centerline defined by the f/4.5 collection optics. In spite of the qualitative nature of these measurements, they serve to identify regions of high temperature soot.

3. RESULTS

The soot volume fraction was calculated from the tomographically inverted extinction measurements using the Lambert-Beer transmissivity law and the Mie extinction formula in the Rayleigh limit [25-27]. An index of refraction $\tilde{m} = 1.57\text{-}0.56i$ was chosen for both HeNe and Ar^+ wavelengths in order to make direct comparisons with the results of Santoro and coworkers [27,28]. Figure 3 shows the symmetrized (averaged about the centerline) steady flame HeNe results; the maximum soot volume fraction is 3.2 ($\pm$ 0.3) x 10^{-7} at H = 60 mm above the fuel tube exit. Above H = 30 mm in the steady flame, peak soot volume fractions determined from the Ar^+ measurements are greater than the HeNe results by ~ 5–10%, which is within the 15% uncertainty estimated for the extinction measurements. Lower in the flame and along the inner edge of the soot profile, Ar^+ extinction yields a significantly larger soot volume fraction

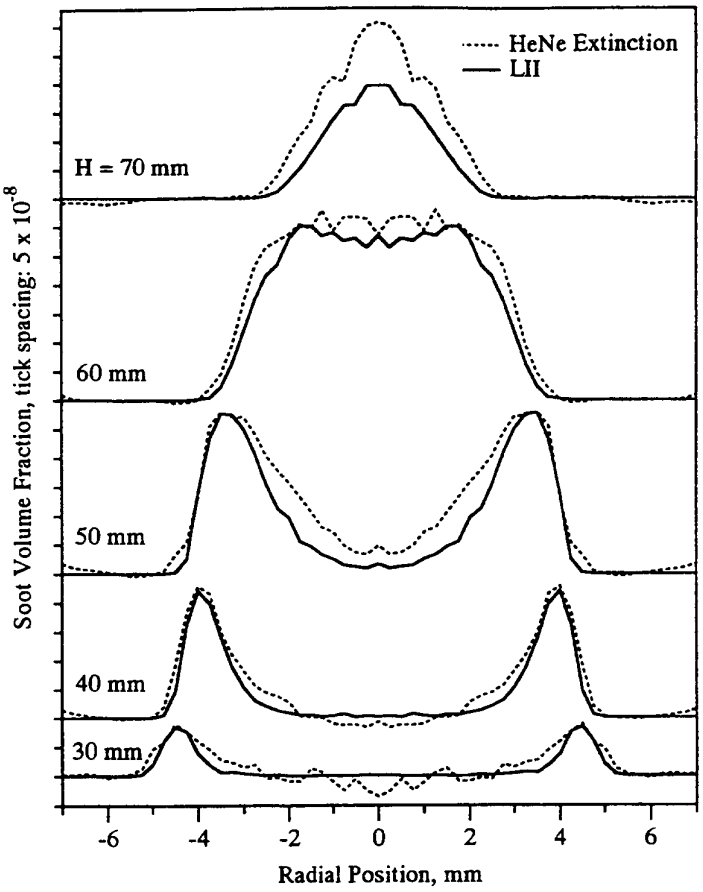

Figure 3. Soot volume fraction from symmetrized HeNe laser extinction (632.8 nm) and laser-induced incandescence (LII) signals at a series of heights in the steady CH_4/air diffusion flame.

than HeNe extinction, consistent with the expectation of greater absorption by PAH in these regions [24,27,29].

Figure 3 also includes the comparison of symmetrized LII signals with the extinction-determined soot volume fractions in the steady methane flame. The peak HeNe soot volume fraction at H = 50 mm was used to calibrate the LII signal, since at this height and radial location one expects the smallest relative contribution of molecular absorption to the observed extinction [29]. The similarity in location and magnitude of the peak values of the extinction and LII results at different heights indicates that the LII signal closely follows the soot volume fraction. Differences in the two signals towards the center of the profiles may be due to significant molecular absorption at 632.8 nm at these locations, as well as the increased error in the tomographic inversion procedure towards the flame centerline [19].

In Fig. 4 the tomographically inverted, time-resolved HeNe extinction data for the flickering flame are shown at heights of 40, 60, 80, and 100 mm above the fuel tube exit. As is evident in this figure, the soot volume fraction measurements higher in the flame exhibit a decreasing time duration of measurable extinction and greater "rippling" noise in the reconstructed annular soot layer. This noise arises from side-to-side flame wobble during the data collection process. The largest instantaneous soot volume fraction (f_v) is 1.3 ($\pm$ 0.3) x 10^{-6}, observed at H = 120 mm; this value is four times greater than the maximum f_v in

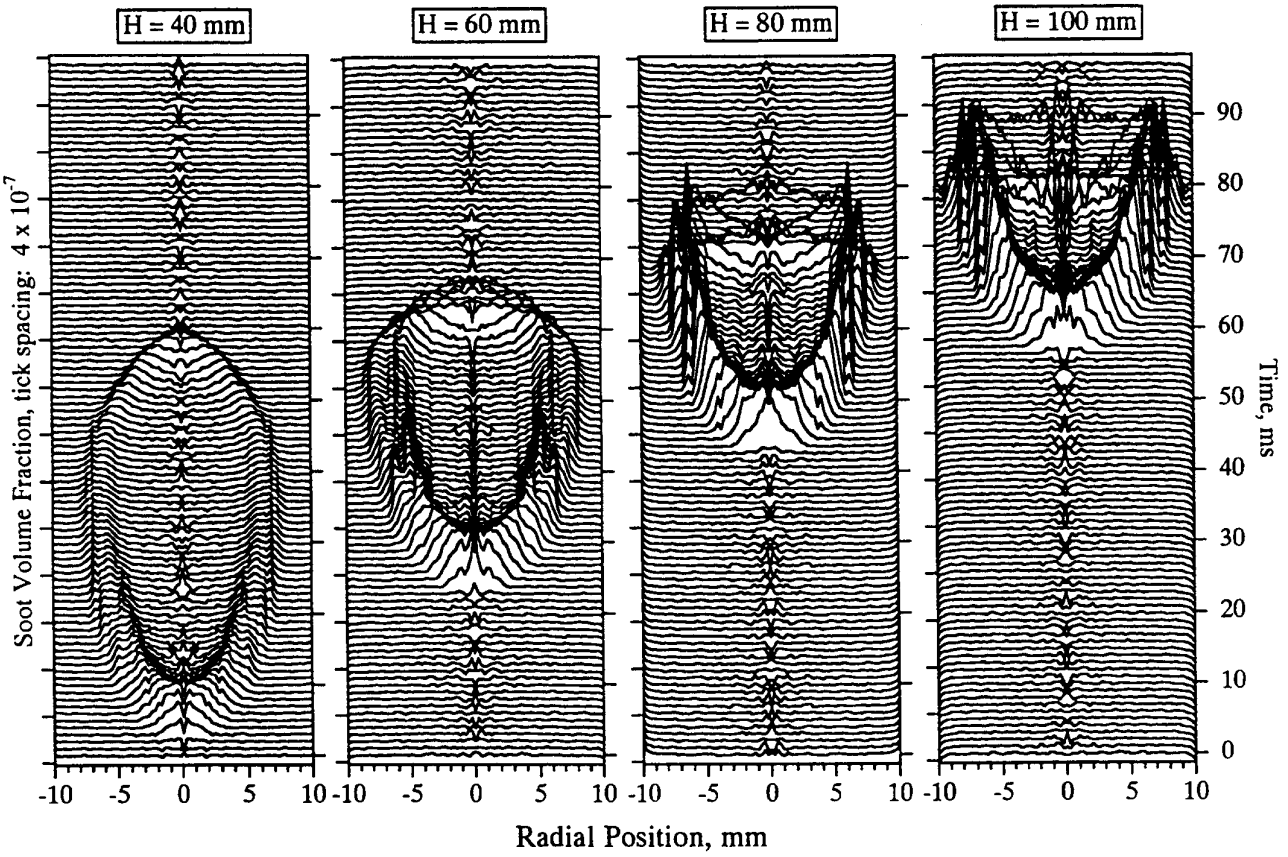

Figure 4. Time evolution of the soot volume fraction field at several heights in the flickering CH_4/air diffusion flame (0.75 V loudspeaker excitation). The soot volume fraction has been computed using a 3-point Abel technique to tomographically invert complete HeNe extinction time records at 0.25 mm spaced radial chords. Each line shown is separated by 1 ms in time and staggered by 6 x 10^{-8} in soot volume fraction. Time progresses from the bottom to the top of the figure, showing first the arrival of soot, the widening of the soot profile into an annular structure as time increases, the convergence of the soot profile to the centerline, and finally its disappearance as the bottom of the clipped-off portion of the flame passes above the measurement location.

the corresponding steady flame. Ar^+ extinction measurements were completed only to H = 100 mm in the flickering flame and yield somewhat greater ($\sim$ 30%) soot volume fractions than the HeNe extinction.

Figure 5 presents the area-integrated and time-averaged (for the flickering flame) soot volume fraction measurements as a function of height. The area under the HeNe flickering flame curve, a volumetric measure of the soot in the flame, is four times greater than its steady counterpart. This figure also shows the consistently larger Ar^+ signals in the flickering flame (up to H = 100 mm) and the convergence of the Ar^+ measurement with the HeNe result higher in the steady flame. As in the steady flame, the increased Ar^+ signals in the flickering flame are attributed to enhanced PAH absorption.

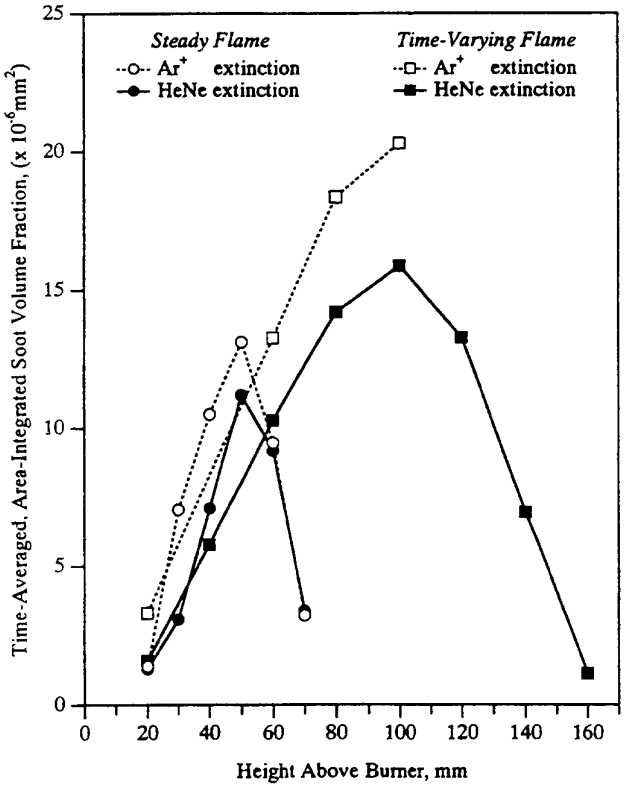

Figure 5. Area-integrated soot volume fraction from symmetrized HeNe (632.8 nm) and Ar^+ (454.5 nm) laser extinction measurements at a series of heights in the CH_4/air diffusion flames. The flickering flame measurements are expressed as time averages over a full cycle period. The area under the steady flame HeNe curve is 3.4×10^{-4} mm^3, and that under the flickering flame is 1.3×10^{-3} mm^3.

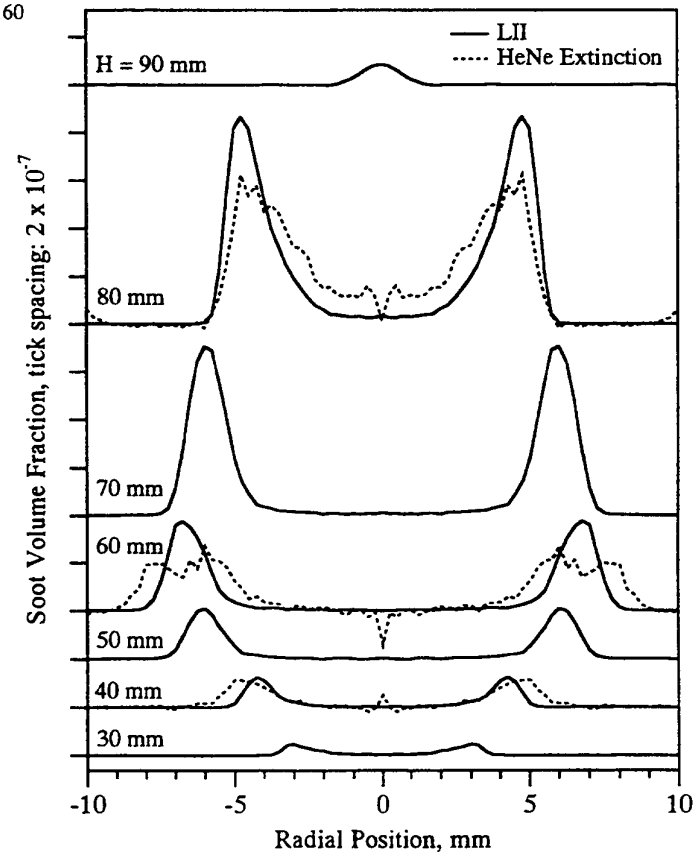

Figure 6. Laser-induced incandescence (LII) signals, interpreted as soot volume fraction, at a series of heights in the flickering CH_4/air diffusion flame at 50% phase. Time-resolved, tomographically inverted HeNe extinction data are also shown at heights of 40, 60, and 80 mm above the burner.

LII signals were measured in the flickering flame up to H = 110 mm for the ten phase angles shown in Fig. 1. The maximum signal gives a soot volume fraction of 1.5 ($\pm$ 0.2) x 10^{-6} at H = 110 mm (80% phase), which is 5 times larger than that observed in the steady flame. Figure 6 shows the symmetrized LII signals compared with the extinction-derived soot volume fraction for 50% phase. Above H = 60 mm in the flickering flame the extinction-derived profiles are generally wider and shorter than their LII counterparts, consistent with the observed flame wobble and the time-averaged nature of the extinction measurement at each radial chord.

Surface plots of the soot scattering signal in the flickering CH_4/air flame are shown in Fig. 7. For vertically polarized incident light the maximum local soot scattering intensity is ~ 8 times greater than that measured in the corresponding steady flame and occurs in the annular soot region of the clipped-off flame for phases of 80 and 90%. At the same locations the enhancement in peak scattering of horizontally polarized light is approximately a factor of 20. Flame tip burnout is complete at about 17 cm in the flickering flame, so it is certainly possible that even greater soot scattering intensities would be found at heights above 13.4 cm, the current limit for imaging.

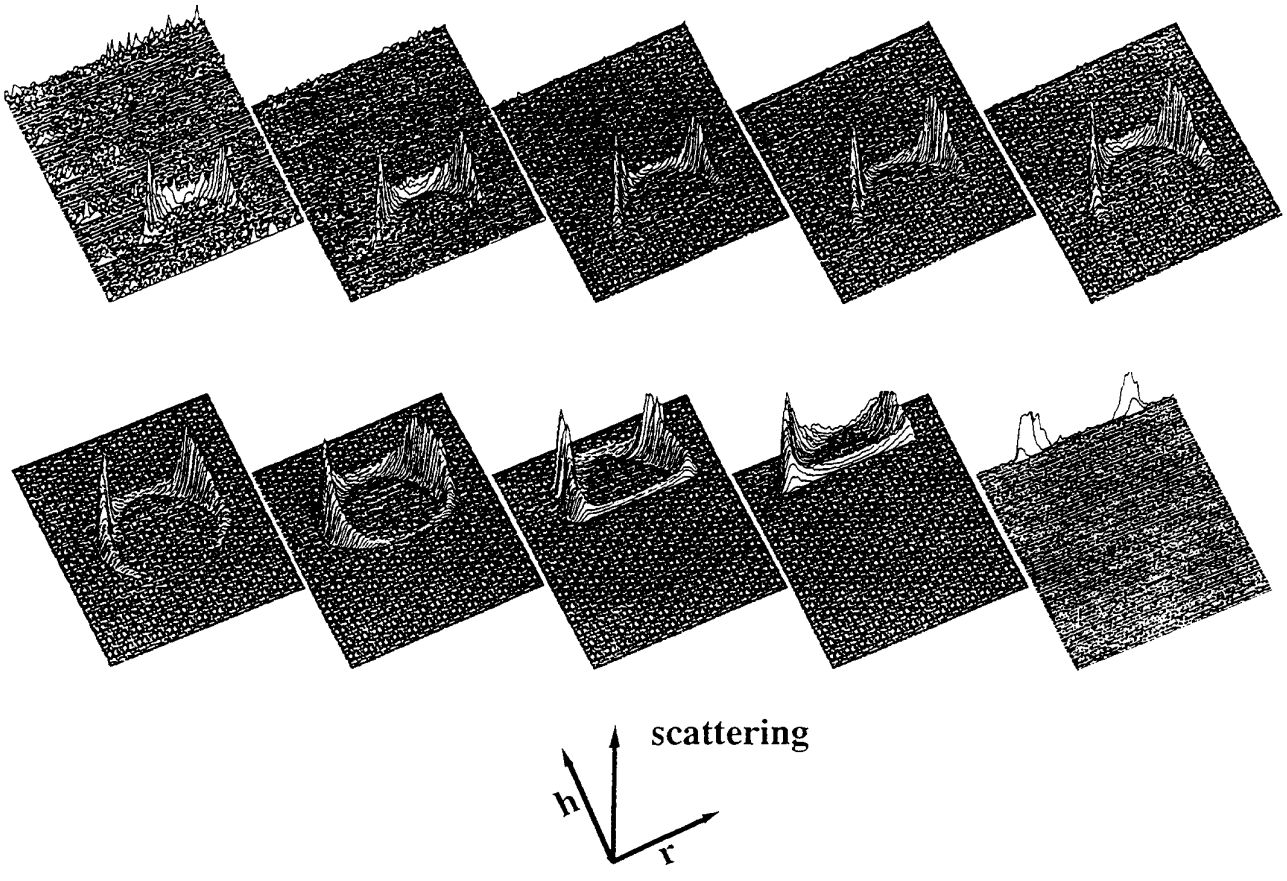

Figure 7. Surface plots of the soot scattering signal from the two-dimensional ICCD images as a function of forcing phase. Each projection corresponds to an image shown in Fig. 1, except that the wavelength of the incident radiation does not coincide with an OH· transition.

Both the broadband PAH fluorescence and the visible flame luminosity are greater in the flickering flame compared to the steady CH_4/air flame. The increase in broadband fluorescence is similar to that observed for the soot volume fraction, but the luminosity enhancement is much smaller. Figures 8 and 9 present measurements from the steady and time-varying flames for the broadband fluorescence and the visible luminosity, respectively. At a phase of 50% in the flickering flame the maximum PAH fluorescence is a factor of four larger than the maximum measured in the steady flame. For our experimental conditions the fluorescence images are most sensitive to the PAH population closest to the high-temperature flame sheet - a region where soot inception occurs [24]. This fluorescence signature may indicate the presence of soot precursors as well as unreactive by-products.

Although the peak soot volume fraction increases by a factor as large as 4-5 in the flickering flame, the maximum visible luminosity is only 50-100% larger and does not occur where the soot loading is greatest. Rather, the strongest luminosity is typically observed at the top and bottom of the clipped-off flame region where the OH• fluorescence and soot scattering signals overlap, indicating vigorous soot oxidation. In contrast, the weak luminosity from the locations of highest soot concentrations suggests that these regions are relatively cool.

Uncertainties quoted for the soot data are one standard deviation, derived from signal variations in repeat measurements of scattering and LII, and those for the extinction measurements are estimated from noise in the profiles. Calibration of LII in the steady flame may lead to small systematic errors for the time-varying flame results, due to changes in soot particle morphology. Long time-scale movements of the flames remain as a possible source of unquantified error.

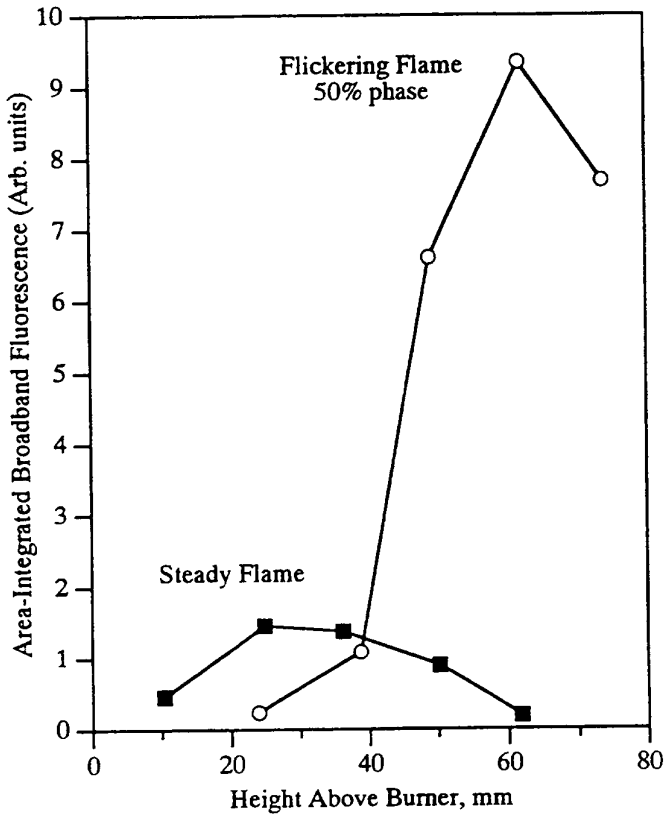

Figure 8. Area-integrated broadband laser-induced fluorescence at a series of heights in the steady and flickering CH_4/air diffusion flames, the latter at 50% phase. The wavelength of the incident radiation is 283.5 nm, and the detection bandpass is 415-550 nm. All data have been obtained at the same laser energy.

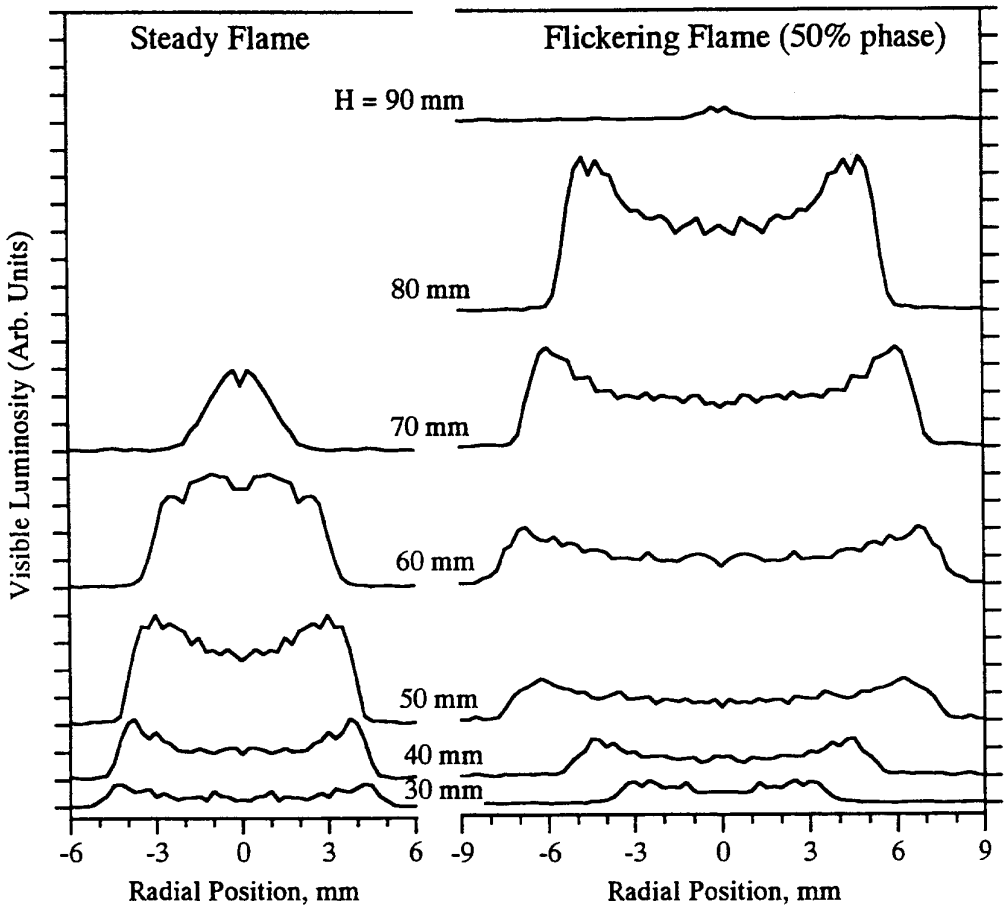

Figure 9. Visible flame luminosity from soot particles at a series of heights in the steady and flickering CH_4/air diffusion flames, the latter at 50% phase. The detection bandpass is 415-550 nm.

4. DISCUSSION

The most important result of our measurements to date on the time-varying CH_4/air diffusion flames is the dramatic enhancement in soot production observed when a steady flame is induced to flicker. This observation may provide a demanding test of the ability of recently formulated integrated soot models [e.g., 30-33] to accurately predict soot formation and oxidation rates in complex combusting flowfields. Changes in residence times, temperatures, and/or local stoichiometries are most likely responsible for the increased soot production. Rayleigh and Mie analyses have been conducted on our scattering and soot volume fraction data in order to estimate the mean soot particle sizes and number densities [13]. Determination of these soot properties is a useful first step in elucidating why soot production is enhanced in the flickering flames.

Table I presents only a small subset of the calculated results: the soot volume fraction (f_v), particle diameter (D), and number densities (N) are given at the point of maximum soot scattering for each

measurement height in the steady flame and in the flickering flame at 50% phase. In lieu of velocity measurements, the contour of maximum scattering is used as a rough guide to the time history of soot particles in the steady flame. The Mie diameters in the steady CH_4/air flame increase up to H = 50 mm, and the calculated number densities decrease slightly as soot particle mass growth occurs, possibly reflecting the effect of soot particle agglomeration. At 50% phase in the flickering flame the derived soot particle diameter increases monotonically with height, while the number densities remain roughly constant until oxidation occurs at the top of the flame. In examining these results, however, recall that any given phase is a snap-shot in the time-history of the flickering flame. Consequently, soot field properties as a function of height do not imply a temporal record of the soot field, as is the case when tracking soot particles along a streamline in the steady flame.

Table I: Mie Analysis of the Soot Field Along the Contour of Maximum Scattering

Height Above Burner	Steady Flame			Flickering Flame (50% phase)		
(mm)	f_v (10^{-7})	D (nm)	N (10^9/cc)	f_v (10^{-7})	D (nm)	N (10^9/cc)
30	0.7 (0.2[a])	39 (5[b])	2.4 (1.3)	0.4 (0.1)	34 (4)	2.0 (1.4)
40	2.2 (0.4)	57 (6)	2.2 (1.1)	1.0 (0.2)	50 (6)	1.5 (0.9)
50	2.3 (0.3)	62 (6)	1.9 (0.8)	2.1 (0.2)	53 (5)	2.7 (1.0)
60	2.2 (0.4)	49 (5)	3.5 (1.8)	3.6 (0.3)	68 (5)	2.2 (0.7)
70	2.0 (0.5)	50 (7)	3.1 (2.2)	6.4 (0.5)	80 (6)	2.4 (0.7)
80				8.1 (0.5)	86 (6)	2.5 (0.7)
90				0.8 (0.2)	85 (11)	0.3 (0.2)

[a] One standard deviation uncertainty estimates.

[b] Diameter and number density uncertainties are the result of propagating soot volume fraction and scattering error estimates through a Rayleigh analysis. These uncertainties agree well with the variation in Mie results over the range of uncertainty in soot volume fraction and scattering values.

The Mie results shown in Table I, when combined with similar trends for all but the greatest heights of the flickering flame, show that particle number densities remain near 2-3 x $10^9/cm^3$ through both the steady and flickering flames, whereas the effective particle diameters increase from a maximum of ~60 nm in the steady flame to ~90 nm in the flickering flame (using $\tilde{m}$ = 1.57-0.56i). Calculations with other values for the index of refraction show the same trends. However, the extent of particle size increase should not be over interpreted, since the particle size parameters ($x = \pi D/\lambda$) in the flickering flame are

large (~ 1) and the deviation between the more accurate fractal agglomerate analysis and a Rayleigh or Mie analysis grows with increasing size parameter [34,35]. Scattering measurements at longer wavelengths, and thus smaller size parameters, would help clarify our analysis.

5. CONCLUSIONS

Quantitative soot volume fraction profiles have been obtained for the first time in a flickering hydrocarbon diffusion flame, using tomographic reconstruction of extinction data obtained at 632.8 nm and calibrated laser-induced incandescence measurements. Both measurements show that the instantaneous, peak soot volume fraction in a flickering CH_4/air flame (with 0.75 V loudspeaker excitation) increases by a factor of 4–5 over the peak soot volume fraction in its steady counterpart. The time-averaged, volume-integrated soot volume fraction also shows a four-fold increase. LII measurements exhibit signal quality superior to laser extinction and appear to track the soot volume fraction accurately. Measurements of the visible flame luminosity provide qualitative information on the location of soot oxidation, and the increased broadband (PAH) fluorescence suggests that higher soot precursor concentrations are present in the flickering CH_4/air flame. A Mie analysis of the soot volume fraction and scattering data suggests that most of the enhanced soot production in the flickering flame results from the formation of larger particles in the time-varying flowfield.

6. ACKNOWLEDGMENTS

We thank Chris Cromer for loaning us the laser power stabilizer and George Mulholland and Robert Santoro for helpful discussions of soot formation processes and diagnostic techniques, particularly with regard to the calibration of LII signals.

7. REFERENCES

1. Smyth, K.C., Harrington, J.E., Johnsson, E.L., and Pitts, W.M., *Combustion and Flame* 95:229-239 (1993).
2. Hamins, A., Yang, J.C., and Kashiwagi, T., *Twenty-Fourth Symposium (International) on Combustion*, The Combustion Institute, Pittsburgh, 1992, pp. 1695-1702.
3. Cetegen, B.M., and Ahmed, T.A., *Combustion and Flame* 93:157-184 (1993).
4. Chen, L.-D., Seaba, J.P., Roquemore, W.M., and Goss, L.P., *Twenty-Second Symposium (International) on Combustion*, The Combustion Institute, Pittsburgh, 1988, pp. 677-684.
5. Davis, R.W., Moore, E.F., Roquemore, W.M., Chen, L.-D., Vilimpoc, V., and Goss, L.P., *Combustion and Flame* 83:263-270 (1991).
6. Ellzey, J.L., and Oran, E.S., *Twenty-Third Symposium (International) on Combustion*, The Combustion Institute, Pittsburgh, 1990, pp. 1635-1640.
7. Buckmaster, J., and Peters, N., *Twenty-First Symposium (International) on Combustion*, The Combustion Institute, Pittsburgh, 1986, pp. 1829-1836.
8. Strawa, A.W., and Cantwell, B.J., *Physics of Fluids* 28, 2317-2320 (1985).
9. Lewis, G.S., Cantwell, B.J., Vandsburger, U., and Bowman, C.T., *Twenty-Second Symposium (International) on Combustion*, The Combustion Institute, Pittsburgh, 1988, pp. 515-522.
10. Pearson, I.G., and Proctor, D., in *Experimental Heat Transfer, Fluid Mechanics, and Thermodynamics 1991* (J.F. Keffer, R.K. Shah, and E.N. Ganic, eds.), Elsevier Science, 1991, pp. 316-322.

11. Vandsburger, U., Seitzman, J.M., and Hanson, R.K., *Combustion Science and Technology* 59:455-461 (1988).
12. Glassman, I., *Twenty-Second Symposium (International) on Combustion*, The Combustion Institute, Pittsburgh, 1988, p. 295 and references therein.
13. Shaddix, C.R., Harrington, J.E., and Smyth, K.C., submitted to *Twenty-Fifth Symposium (International) on Combustion.*
14. Norton, T.S., Smyth, K.C., Miller, J.H., and Smooke, M.D., *Combustion Science and Technology* 90:1-34 (1993).
15. Smooke, M.D., editor, *Reduced Kinetic Mechanisms and Asymptotic Approximations for Methane-Air Flames*, Lecture Notes in Physics Vol. 384, Springer-Verlag, Berlin (1991).
16. Puri, R., Santoro, R.J., and Smyth, K.C., *Combustion and Flame*, in press.
17. Miller, J.H., Mallard, W.G., and Smyth, K.C., *Combustion and Flame* 47:205-214 (1982).
18. Montgomery, G.P. and Reuss, D.L. *Applied Optics* 21:1373-1380 (1982).
19. Dasch, C.J., *Applied Optics* 31:1146-1152 (1992).
20. We thank J. Houston Miller for providing us with the base Pascal algorithm required to tomographically invert extinction records in time or frequency.
21. Dec, J.E., zur Loye, A.O., and Siebers, D.L., *SAE Technical Papers Series* SAE-910224, Society of Automotive Engineers, PA, 1991.
22. Tait, N.P., and Greenhalgh, D.A., *Proceedings of the "Optical Methods and Data Processing in Heat Transfer and Fluid Flow" Conference*, London, April 1992.
23. Quay, B., Lee, T.-W., and Santoro, R.J., *Combustion and Flame*, in press.
24. Smyth, K.C., Miller, J.H., Dorfman, R.C., Mallard, W.G., and Santoro, R.J., *Combustion and Flame* 62:157-181 (1985).
25. Kerker, M., *The Scattering of Light*, Academic Press, New York, 1969, pp. 31-39.
26. D'Alessio, A., in *Particulate Carbon: Formation During Combustion* (D.C. Siegla and G.W. Smith, Eds.), Plenum, New York, 1981, pp. 207-259.
27. Santoro, R.J., Semerjian, H.G., and Dobbins, R.A., *Combustion and Flame* 51:203-218 (1983).
28. Richardson, T.F., and Santoro, R.J., private communication, 1993.
29. Prado, G., Garo, A., Ko, A., and Sarofim, A., *Twentieth Symposium (International) on Combustion*, The Combustion Institute, Pittsburgh, 1984, pp. 989-996.
30. Syed, K.J., Stewart, C.D., and Moss, J.B., *Twenty-Third Symposium (International) on Combustion*, The Combustion Institute, Pittsburgh, 1990, pp. 1533-1541.
31. Leung, K.M., Lindstedt, R.P., and Jones, W.P., *Combustion and Flame* 87:289-305 (1991).
32. Honnery, D.R., and Kent, J.H., *Twenty-Fourth Symposium (International) on Combustion*, The Combustion Institute, Pittsburgh, 1992, pp. 1041-1047.
33. Villasenor, R., and Kennedy, I.M., *Twenty-Fourth Symposium (International) on Combustion*, The Combustion Institute, Pittsburgh, 1992, pp. 1023-1030.
34. Charalampopoulos, T.T., and Chang, H., *Combustion and Flame* 87:89-99 (1991).
35. Mountain, R.D., and Mulholland, G.W., *Langmuir* 4:1321-1326 (1988).